Geosci. Model Dev., 17, 1651–1665, 2024
https://doi.org/10.5194/gmd-17-1651-2024

Geoscientific Model Development
Open Access
EGU

Parameter estimation for ocean background vertical diffusivity coefficients in the Community Earth System Model (v1.2.1) and its impact on El Niño–Southern Oscillation forecasts

Zheqi Shen[1,2,4], **Yihao Chen**[2], **Xiaojing Li**[3,4], **and Xunshu Song**[3,4]

[1]Key Laboratory of Marine Hazards Forecasting, Ministry of Natural Resources, Hohai University, Nanjing, China
[2]College of Oceanography, Hohai University, Nanjing, China
[3]State Key Laboratory of Satellite Ocean Environment Dynamics, Second Institute of Oceanography, Ministry of Natural Resources, Hangzhou, China
[4]Southern Laboratory of Ocean Science and Engineering (Zhuhai), Zhuhai, China

Correspondence: Zheqi Shen (zqshen@hhu.edu.cn)

Received: 4 June 2023 – Discussion started: 31 July 2023
Revised: 16 January 2024 – Accepted: 19 January 2024 – Published: 26 February 2024

Abstract. This study investigates parameter estimation (PE) to enhance climate forecasts of a coupled general circulation model by adjusting the background vertical diffusivity coefficients in its ocean component. These parameters were initially identified through sensitivity experiments and subsequently estimated by assimilating the sea surface temperature and temperature–salinity profiles. This study expands the coupled data assimilation system of the Community Earth System Model (CESM) and the ensemble adjustment Kalman filter (EAKF) to enable parameter estimation. PE experiments were performed to establish balanced initial states and adjusted parameters for forecasting the El Niño–Southern Oscillation (ENSO). Comparing the model states between the PE experiment and a state estimation (SE) experiment revealed that PE can significantly reduce the uncertainty of these parameters and improve the quality of analysis. The forecasts obtained from PE and SE experiments further validate that PE has the potential to improve the forecast skill for ENSO.

1 Introduction

The coupled general circulation model (CGCM) is a prominent tool that is widely utilized for predicting future climate. However, limitations arise in simulations and forecasts derived from CGCMs due to imperfections in model physics, numerical schemes, and initial conditions. Coupled data assimilation, referred to as state estimation (SE), can enhance the accuracy and consistency of initial conditions in CGCMs by integrating coupled models with available observation data. SE is commonly employed in current operational forecasting systems (Stammer et al., 2016; Balmaseda et al., 2009). In addition to SE, researchers have developed parameter estimation (PE) or parameter optimization (PO) methods to mitigate model errors arising from uncertainties in empirical parameters of diverse physical parameterization schemes. These methods optimize model parameters using observation data, leading to a substantial reduction in model errors (Evensen et al., 1998; Zhang et al., 2020).

Recent studies have shown the potential of PE to enhance forecast accuracy (Wu et al., 2012; Zhang et al., 2012) by reducing model biases (Tong and Xue, 2008a, b). For instance, PE experiments have been performed using conceptual models (Han et al., 2013), intermediate-complexity models (ICMs) (Wu et al., 2016), and CGCMs (Liu et al., 2014a) to illustrate the capacity of PE to address model errors and enhance the predictability of climate and weather events. However, most of these studies were carried out under perfect model scenarios, and only a limited number of studies have estimated parameters using real observation data. PE presents various challenges in real-world scenarios, including inconsistencies in initial conditions, biases in numerical

models compared to reality, and difficulties in determining the ideal value of unknown parameters (Zhao et al., 2019).

Despite these challenges, several examples of PE in actual forecast models exist. For example, Menemenlis et al. (2005) used Green's function approach to estimate parameters in an ocean general circulation model, demonstrating improved estimations compared to the prior values. Hu et al. (2010) performed parameter estimation in a weather model, confirming that optimized parameters can improve the model's forecast accuracy for real-world weather events. Kondrashov et al. (2008) used observation data to estimate parameters in a simplified ICM, verifying that optimized parameters can better match observation results. Similarly, Zhao et al. (2019) and Gao et al. (2021) performed parameter estimation in the Zebiak–Cane model, another ICM, using real observations. They both revealed that prediction skills for the El Niño–Southern Oscillation (ENSO) were improved with the estimated parameters.

There are still challenges when utilizing PE with observation data in CGCMs for the purpose of improving forecasts and reanalysis (Zhang et al., 2020). To overcome these challenges, we employed the improved PE method proposed by Shen and Tang (2022) in this study to estimate background vertical diffusivity coefficients in the ocean model via PE experiments. A coupled data assimilation system that is built upon the Community Earth System Model (CESM) and the ensemble adjustment Kalman filter (EAKF) method (Anderson, 2003) is used in this study. Specifically, we assimilated various ocean observation data, such as satellite sea surface temperature (SST) and temperature–salinity (T–S) profile data, to provide optimal parameters for seasonal forecasting. Additionally, we used the results obtained from PE to initialize ENSO forecasting; these results were subsequently compared to SE initialization results to illustrate the advantages of PE in enhancing the CGCM's ENSO-forecasting ability.

The paper is organized as follows: Sect. 2 introduces the data assimilation system, observation data, PE method, and experimental settings. Section 3 presents the results of the sensitivity experiment while comparing the analyses and forecasts using PE and SE. Lastly, Sect. 4 concludes the study.

2 Data assimilation system and PE methods

It has been demonstrated that coupled models can provide more compatible initial conditions via coupled data assimilation (Fujii et al., 2009; Mulholland et al., 2015; Penny and Hamill, 2017), which, in turn, improves seasonal predictions (Jin et al., 2008; Kug et al., 2008). In a previous study, we developed a coupled assimilation and ensemble forecasting system based on the fully coupled model CESM (Chen et al., 2022). The system employed the EAKF method to assimilate ocean observations from various sources and adjust the state variables of the ocean model, thereby influencing other model components through flux exchanges in the coupled process. Notably, the assimilation results have demonstrated significant improvement in terms of ENSO-forecasting skill (Chen et al., 2023). In the current study, we extended this system by incorporating a parameter estimation function, which enabled the estimation of several critical parameters in the ocean model.

2.1 The CESM model and the background vertical diffusivity coefficients

The study utilized version 1.2.1 of the open-source global coupled model CESM, developed by the National Center for Atmospheric Research (NCAR). This integrated model includes the Community Atmospheric Model version 4 (CAM4) (Neale et al., 2010), the Parallel Ocean Program version 2 (POP2) (Danabasoglu et al., 2012), the Community Ice Code version 4 (CICE4), and the Community Land Model version 4 (CLM4), as well as other modules. The atmospheric component has a horizontal resolution of $0.9^\circ \times 1.25^\circ$ with 26 vertical levels, while the ocean component was integrated at a nominal resolution of 1° with an enhanced meridional resolution of 0.5° in the equatorial region and 60 vertical levels.

In many OGCMs, vertical mixing can be parameterized separately by region, including upper-boundary-layer schemes and a diapycnal-mixing scheme for the ocean interior. The K-profile parameterization (Large et al., 1994) is widely used to parameterize vertical mixing in ocean models. It includes a background diffusivity parameter that determines the diapycnal mixing in the thermocline. It is critical to the heat transfer between the upper boundary layer and the ocean interior. The background diffusivity parameter is typically set to a constant value, and its magnitude is determined by fitting the model to observations or theoretical considerations. As identified by much of the previous work, the background diffusivity parameterization is a key factor in vertical mixing parameterizations, and it has significant uncertainties and contributes to a large bias in SST simulations (Jochum, 2009). Zhu and Zhang (2018) have shown that a better background diffusivity parameterization leads to more realistic simulations of the cold tongue and equatorial thermocline, which has the potential to affect the fidelity of simulated seasonal to interannual variability in the tropical Pacific, such as the ENSO phenomenon. Therefore, the present study focused on estimating the parameters in background diffusivity parameterization.

The ocean model of CESM, POP2, was initially proposed by Smith et al. (1992) to solve three-dimensional ocean dynamic primitive equations on a global grid under the assumptions of Boussinesq and hydrostatic approximation. The background diffusivity parameter, denoted as k_w, is mainly used to characterize mixing processes resulting from the breaking of inertial internal waves (Smith et al., 2010). However, due to the uncertain propagation and dissipation behav-

ior of these waves, the parameter value of k_w has significant uncertainty. Munk (1966) first estimated the averaged diapycnal diffusivity of $10^{-4}\,m^2\,s^{-1}$ based on the advective–diffusive balance, thus requiring a background diffusivity of $O(10^{-4}\,m^2\,s^{-1})$ to realistically produce the pycnocline in numerical models (Bryan, 1987). However, microstructure measurements generally give estimates that can be reduced by 1 order of magnitude (Gregg, 1977; Ledwell et al., 1998). Hence, a constant background diffusivity of $O(10^{-5}\,m^2\,s^{-1})$ has typically been applied in many ocean and climate modeling studies. Recently, observational evidence has indicated that the assumed constant background diffusivity is not uniform but rather is spatially varying (Kunze et al., 2006). In particular, microstructure measurements suggest that background diffusivity should be reduced near the Equator, with a magnitude of $O(10^{-6}\,m^2\,s^{-1})$ (Cheng and Kitade, 2014; Gregg et al., 2003). Jochum (2009) adopted a latitudinal structure of k_w in the POP2 model and found that it simulated the ocean state better, which has been subsequently accepted by follow-up studies. Specifically, POP2 utilizes four independent background vertical diffusivity coefficients (BVDCs) to simulate the latitudinal structure of the background diffusivity. Table 1 lists each coefficient's default values and descriptions (Smith et al., 2010).

The BVDCs have a total of four constants, comprising a coefficient v_1 describing global diffusivity, a coefficient v_e describing equatorial diffusivity (Gregg et al., 2003), a coefficient v_p describing the diffusivity near latitudes of 28.9° S and 28.9° N, and a coefficient v_b describing diffusivity in the Banda Sea region alone (Jochum and Potemra, 2008). Among them, v_p is also known as the maximum PSI-induced diffusivity, representing the result of the parametric subharmonic instability (PSI) of the M2 tide (MacKinnon and Winters, 2005). Therefore, in POP2, the background diffusivity parameter k_w has only a fixed form of spatial variation (Smith et al., 2010). Except for the Banda Sea, which takes on a specific value, globally, k_w varies only latitudinally and can be expressed as follows:

$$k_w = v_e + v_1\left(\frac{\theta}{10}\right)^2 + v_p e^{-0.4(\theta+28.9)} + v_p e^{-0.4(\theta-28.9)}, \quad (1)$$

where θ is the latitude.

Therefore, the k_w value has been modified from its typically constant value of 0.1 to $0.17\,cm^2\,s^{-1}$ ($v_1 + v_e = 0.17$) almost everywhere in POP2, and there are regions where different values are used: $1.0\,cm^2\,s^{-1}$ in the Banda Sea (v_b), $0.3\,cm^2\,s^{-1}$ in the latitude bands around 28.9° N and S ($v_1 + v_e + v_p$), and $0.01\,cm^2\,s^{-1}$ at the Equator (v_e).

2.2 The data assimilation and ensemble prediction system

The Data Assimilation Research Testbed (DART) was employed in this study to implement the data assimilation system (Anderson et al., 2009; Karspeck et al., 2018). DART, an open-source software, offers various filter methods' implementations. Previously, this data assimilation system was used to study the impact of initial-state errors on assimilation quality by assimilating ocean observations within a quasi-weakly coupled data assimilation framework (Chen et al., 2022). The EAKF method yielded the analysis ensemble, serving as the initial condition for climate variability forecasting. Notably, the system's initial conditions facilitated the forecasting of significant climate variability, such as ENSO and IOD (the Indian Ocean dipole), and consequently directed a demonstrable improvement in forecasting skill (Chen et al., 2023).

The description of the assimilation system is presented in detail by Chen et al. (2022). In brief, it is a weakly coupled data assimilation system since only ocean observations are assimilated, and the coupled model is used for integration. This study utilizes the ensemble adjustment Kalman filter approach with 20 ensemble members. The ensemble members are constructed using long-term spin-up integration results and then repeatedly assimilating the WOA18 (Garcia et al., 2019) climatology data over 4 years to correct the climatological bias. This approach is essential to ensure that the initial ensemble can effectively incorporate all observations during the data assimilation procedure.

Two sets of observation data are assimilated every 10 d. One dataset is the Optimum Interpolation Sea Surface Temperature (OISST) dataset version 2.1 retrieved from the National Oceanic and Atmospheric Administration (NOAA). The other is the EN4 profile dataset version 4.2.1 of the UK Met Office. The OISST dataset has a daily 0.25° resolution and was constructed by combining observations from different platforms (satellites, ships, buoys, and Argo floats) on a regular global grid. The EN4 profile dataset is a collection of ocean temperature and salinity (T–S) profiles obtained across global oceans from 1900 to the present. Quality control methods ensure good quality (Gouretski and Reseghetti, 2010).

The datasets were pre-processed before being assimilated into the system. Regarding the data assimilation system that assimilates SST and T–S profiles every 10 d, daily profiles were merged and assigned to the final day of each sequence. To prevent overfitting due to assimilating excessive profile observations, the data at different depths were first interpolated to 31 layers from 5 m to approximately 2100 m and then averaged horizontally. Specific vertical depths were obtained from the EN4 analysis data (Good et al., 2013). The mean value of all the data in each $1° \times 1°$ cell at each level was regarded to be the observation value. Moreover, the OISST data were thinned such that only data on the $1° \times 1°$ grids

Table 1. Background vertical diffusivity coefficients (BVDCs) of KPP parameterization in POP2.

Name list variable	Parameter description	Default value ($m^2\ s^{-1}$)	Notations
bckgrnd_vdc1	Background diffusivity	0.16	υ_1
bckgrnd_vdc_eq	Equatorial diffusivity	0.01	υ_e
bckgrnd_vdc_psim	Maximum PSI-induced diffusivity	0.13	υ_p
bckgrnd_vdc_ban	Banda Sea diffusivity	1.0	υ_b

were assimilated every 10 d. Previous studies have shown that this processing method can produce effective state estimation results (Chen et al., 2022, 2023).

Localization was employed using the Gaspari and Cohn function (Gaspari and Cohn, 1999), which employed a cut-off half-width of 0.1 rad (approximately 600 km) for both observations. The SST and T–S profiles had vertical localization half-widths of 250 and 1000 m, respectively. Additionally, the application of covariance inflation involved utilizing a constant inflation factor with $\alpha = 1.02$ for model states. These factors were determined empirically and verified in prior studies (Shen and Tang, 2022; Chen et al., 2022, 2023).

2.3 Parameter estimation method

One approach to achieving PE is the state vector augmentation method, in which parameters are treated as specific model variables and included in the state vectors. By updating the augmented state vector with observations, the model state and parameters can be estimated concurrently (Kivman, 2003; Annan and Hargreaves, 2004; Annan, 2005). Applying PE in a CGCM presents several technical challenges. Firstly, many parameters in the GCM emanate from simplifying underlying physical processes, which may display globally uniform values. Updating a few global parameters with numerous data may lead to an accumulation of sample errors, leading to PE failure. Since the parameters estimated in this paper are four constants, this is the main challenge in the experiments. To overcome this hurdle, we used the adaptive spatial averaging (ASA) method designed by Liu et al. (2014b) for the CGCM. In each data assimilation step, we transformed each parameter from a single scalar value into a two-dimensional field, considering spatial dependence and localization during the assimilation. Afterward, we use the adaptive algorithm to average the two-dimensional parameter fields to produce a scalar value incorporated into subsequent model integration. This algorithm calculates the ratio of the a posteriori standard deviation to the a priori standard deviation at each grid point after each update of the two-dimensional parameters, which implies the strength of the effect of assimilation, and then averages the parameter values at grid points where the ratio exceeds a certain threshold. This threshold is chosen using an adaptive algorithm to ensure that a certain number of grid points (in this experiment, 10 000 out of a total of 80 000 grids) are included in the calculation of the averaged parameters. For more details, refer to Shen and Tang (2022).

A further challenge arises from covariance inflation. Studies have noted that the parameter ensemble's spread (standard deviation) is generally relatively lower than that of the state ensemble, primarily because parameters remain constant for the mode integration. Consequently, ensemble-Kalman-filter-based PE requires a larger covariance inflation factor for the parameter ensemble. In a previous study, we employed twin experiments to demonstrate the necessity of covariance inflation for PE of BVDCs in CESM and developed a two-stage covariance inflation approach (Shen and Tang, 2022). Specifically, the conventional covariance inflation was applied to the augmented vector of the model states and the 2-D parameter fields using a fixed inflation factor of $\alpha = 1.02$ before assimilation. Afterward, we average the analysis data of 2-D parameter fields to obtain global scalars and utilize a covariance inflation factor of $\alpha_p = 1.25$ solely for the parameter ensemble. This factor is deduced by calculating the average growth rate of the state variables in the model integration. Figure 1 provides a schematic diagram illustrating the PE process described above.

However, the conditional covariance inflation (CCI) method is usually used in practical data assimilation to ensure that the ensemble spread does not fall below a lower bound (Aksoy et al., 2006; Liu et al., 2014a). The CCI is designed to inflate the parameter ensemble spread back to a predefined threshold value when it is smaller than the threshold. In this work, we intentionally do not use the CCI method and let the parameter ensemble degenerate after several data assimilation cycles. After that, all ensemble members use the same improved parameters that no longer change value with the subsequent data assimilation. This strategy allows the parameter ensemble to converge and makes subsequent ensemble forecasting experiments easier to implement.

It is also worth noting that, in order to avoid unphysical parameter values, after each parameter estimation, if an abnormal parameter value (e.g., negative value) occurs for an ensemble member, we remove the parameter and use the parameter of the neighboring member to integrate the model.

2.4 Experimental design and verification data

Conducting sensitivity analyses (Navon, 1998) before PE is necessary to ensure that the parameters have a significant im-

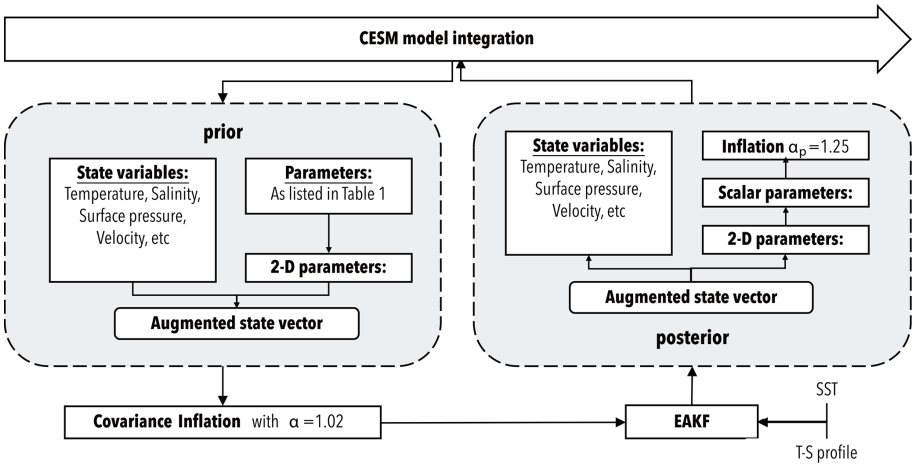

Figure 1. Schematic diagram of the parameter estimation process in the CESM model.

pact on the observed variables. In this study, the sensitivity experiment was initially conducted to show the sensitivity of model temperature and salinity to the BVDCs. An ensemble of size 20 was integrated using the same initial states but with perturbed parameters. We perturbed each BVDC by adding noise generated from a Gaussian distribution with a mean value of 0 and a standard deviation of 30 % of its default value. We measured the variable sensitivity to the perturbed parameters by using the ensemble spread of each variable.

Subsequently, we conducted separate SE and PE experiments using the initial ensemble introduced earlier. The assimilation time window started in January 2005 and continued until December 2017. In the SE experiment, the SST and T–S profiles were assimilated every 10 d to update the model state variables that include temperature, salinity, sea surface pressure, and surface current velocity. The BVDCs listed in Table 1 were used in model integration during the entire period. The PE experiment used the same observations to update the model state variables and the BVDCs concurrently. As Zhang et al. (2012) showed, the signal-to-noise ratio of the state–parameter error covariance in the coupled model can be significantly improved after the state estimation reaches quasi-equilibrium. Therefore, we performed only pure state estimation in the first year of the PE experiment and activated the PE function from the beginning of the second year. That is, the parameter values changed gradually from 2006 onwards. At this point, the observation-constrained states can improve the parameter estimates more effectively.

We compared the results of SE and PE experiments with validation data to demonstrate the impact of PE on reducing analysis errors. The temperature and salinity from the objective analysis data of EN4.2.1 (Good et al., 2013) are used for validation. It should be noted that the EN4 profile dataset for assimilation is a collection of profiles, and the EN4 objective analysis dataset is processed and gridded data. To ensure impartiality in the validation data, we also incorporated high-quality reanalysis products such as the Ocean Reanalysis System 4 (ORAS4) by Balmaseda et al. (2013) and the Geophysical Fluid Dynamics Laboratory's ensemble coupled data assimilation (GFDL/ECDA) by Zhang et al. (2007).

The EAKF can provide initial conditions for ensemble prediction by running an ensemble of members. The analysis ensembles of SE and PE experiments were utilized as initial conditions for climate forecasting with the coupled model. We conducted ensemble forecast experiments from 2008 to 2017 using the analysis ensembles derived from both SE and PE. The parameters obtained by PE were also employed in the latter case. Predictions were issued at the beginning of each January, April, July, and October, extending for 12 months. The Hadley Centre sea ice and sea surface temperature dataset (HadISST) (Rayner et al., 2003) served as a reference dataset to compare the produced prediction products.

The schematics in Fig. 2a–c show the sensitivity experiment, the SE experiment, and the PE experiment, respectively. It can be seen that the sensitivity experiment is a free-integration experiment using the same initial condition and different parameters. The SE experiment uses the ensemble of state variables and the same default parameters. At the same time, the PE experiment uses ensembles for both state variables and parameters. PE experiments are divided into three phases, which we will specify in the "Results and discussions" section. Moreover, it also shows that the state and parameter estimation results are used in the later hindcast experiments.

3 Results and discussions

3.1 Sensitivity experiment

Twenty identical ensemble members were utilized for the parameter sensitivity experiment in the CESM integration,

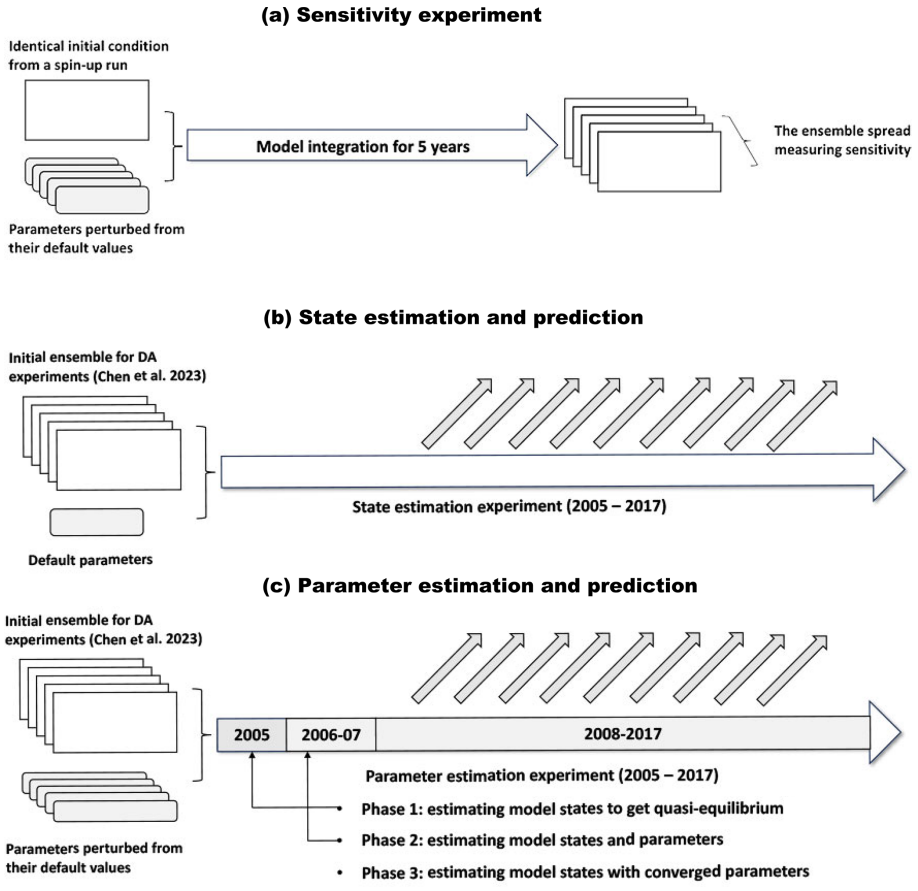

Figure 2. The schematic diagrams of **(a)** the sensitivity experiment, **(b)** the state estimation and prediction experiment, and **(c)** the parameter estimation and prediction experiment.

which persisted for 5 years, with four parameters perturbed simultaneously. It is worth noting that we tried experiments where we perturbed the parameters one by one, and the experimental results showed that perturbing the different BVDCs had a comparable effect (not shown here), so we used this simultaneous perturbation scheme. The ensemble spreads of temperature and salinity variables, which measure their sensitivity to the perturbed parameters, are shown in Fig. 2. The global (66.5° S–66.5° N) and equatorial (5° S–5° N) averaged temperature and salinity ensemble spreads were demonstrated accordingly. Perturbing BVDCs in the model leads to a rapid increase in temperature and salinity ensemble spread within the first year, followed by relative stability in the succeeding years. Figure 3 shows that temperature variables have the maximum sensitivity to BVDCs at approximately 100 m depth, with salinity variables being most sensitive to these parameters at the sea surface. The influence of parameter uncertainty can extend up to a depth of approximately 400 m. Additionally, the equatorial area is highly sensitive to BVDC parameters in terms of temperature at a depth of 50–100 m and in terms of salinity at the sea surface. The surface temperature variability in Fig. 3a shows a conspicuous seasonal cycle which can possibly be related to the diverse rates of change in mean temperature instigated by distinct ocean areas between the Northern Hemisphere and the Southern Hemisphere.

The last 3 years' outcomes were used to compute the mean spread and analyze its spatial distribution. Figure 4 provides additional validation that temperature variability is highest within the equatorial range and most pronounced at a depth of 100 m. In deeper layers, the parameters affect the temperature more significantly in the western Pacific. Additionally, salinity is highly sensitive to the parameters in the warm-pool region of the tropical western Pacific, and the sensitivity of salinity to parameters is highest in the shallow layers of less than 50 m depth. Furthermore, in the extratropics, the temperature and salinity in the Kuroshio Extension and Gulf Stream regions are also sensitive to these parameters to some extent.

The sensitivity experiment shows that the model temperature and salinity are sensitive to the uncertainty in the BVDCs, strongly indicating that assimilating SST and T–S profiles can potentially reduce the uncertainty.

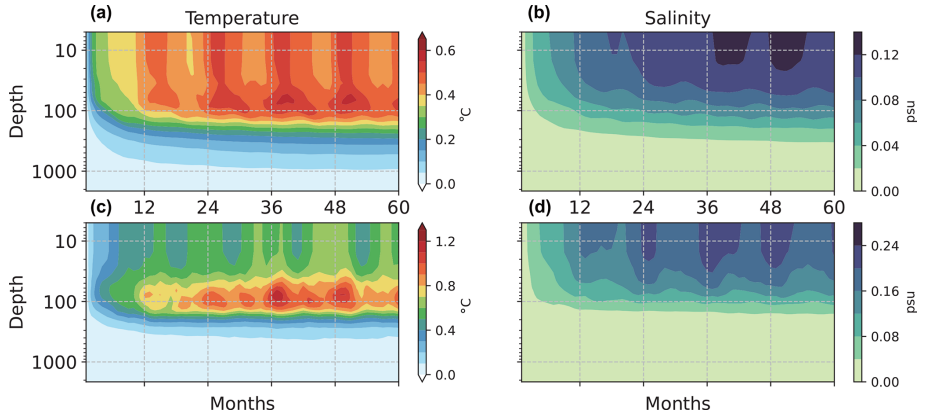

Figure 3. The global averaged (between 60° S and 60° N) ensemble spread of temperature **(a)** and salinity **(b)**; **(c)** and **(d)** are the same as **(a)** and **(b)** but were averaged over the Equator (between 5° S and 5° N).

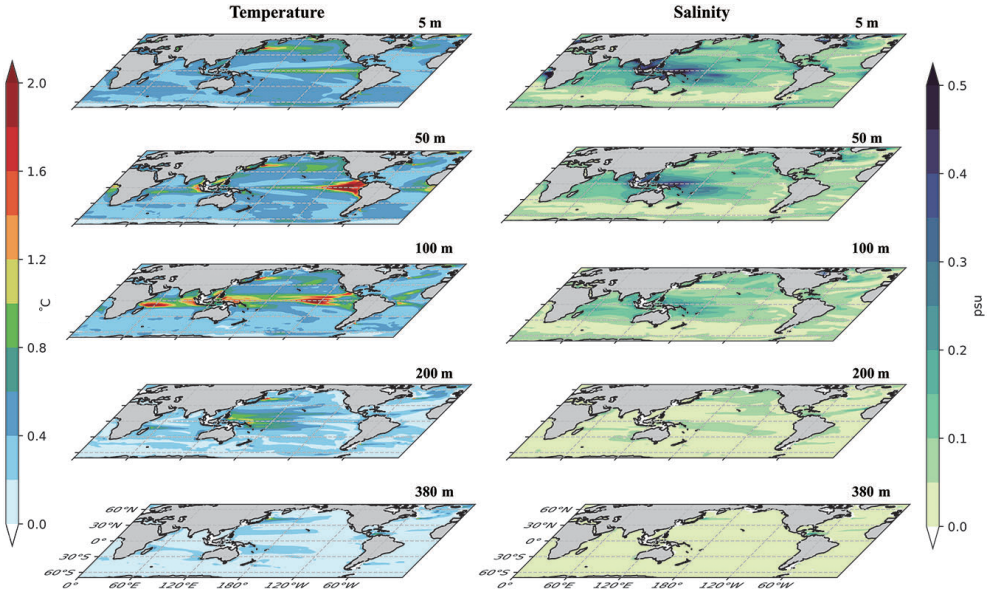

Figure 4. Spatial distribution of the ensemble spread of sea temperature (left) and salinity (right) at different depths.

3.2 Estimated parameters

We conducted separate SE and PE experiments, assimilating observations during the period between January 2005 and December 2017. In the SE experiment, default values of the BVDCs were consistently used in all ensemble members throughout the entire period. However, the PE experiment comprised three distinct phases. During the initial phase, we utilized perturbed parameters to perform state estimation. It spans a period of 1 year and brings the state estimation process to approximately quasi-equilibrium, where the uncertainty of coupled model states is sufficiently constrained by observations. In the second phase, spanning from 2006 to 2007, we activated the PE function illustrated in Fig. 1. This function facilitated continuous correction of the parameter ensemble through observations. Finally, during the third phase, spanning from 2008 to 2017, these parameters remained unchanged.

Figure 5 depicts a graphical representation of the 20 ensemble members of the four BVDCs over time, with the ensemble mean represented by the solid red line. Observations gradually decreased the spread of the parameter ensemble, resulting in less uncertainty. After approximately 2 years, the parameter ensemble degenerated, and the spread reached 0. Consequently, assimilating observations could no longer adjust the parameters.

Table 2 presents the final values of BVDCs. Notably, v_1 and v_p values are 20 % higher than the default values, while v_b is 10 % higher (except for v_e, which is slightly lower than the default value). It is also worth noting the almost globally increasing value of the background vertical diffusivity, k_w, as calculated through Eq. (1) and depicted in Fig. 6. The

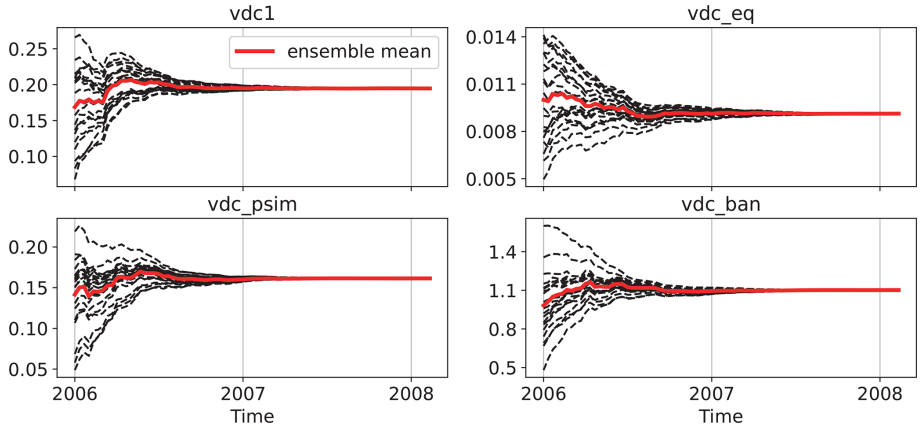

Figure 5. Evolution of each parameter since 2006, in which the solid red lines indicate the ensemble mean.

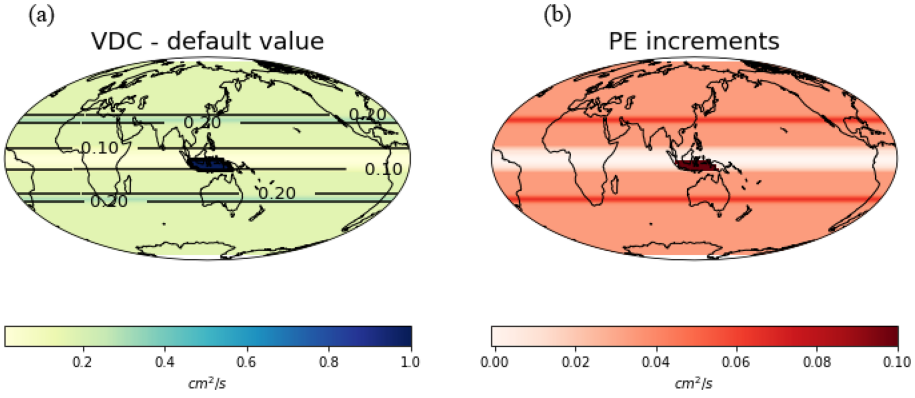

Figure 6. (a) Default latitudinal structure of background vertical diffusivity; **(b)** the increment of the background vertical diffusivity from PE.

Table 2. PE final BVDC values.

Parameters	v_1	v_e	v_p	v_b
Default value ($m^2\ s^{-1}$)	0.16	0.01	0.13	1.0
PE final value ($m^2\ s^{-1}$)	0.195	0.0091	0.161	1.10
Ratio of increase	21.9 %	−9 %	23.8 %	10 %

left-hand side of Fig. 6 displays the band structure of the default background diffusivity, while the increment obtained by PE is shown on the right-hand side, further validating the achieved results.

3.3 Quality of the analysis

As previously mentioned, the parameters have remained unchanged since 2008. Consequently, the third phase of the PE experiment can be considered to be a distinct SE experiment using the estimated parameters listed in Table 2. This study focuses specifically on evaluating the analyses obtained from the third phase by comparing the results of the PE and SE experiments.

We compare our analysis fields to the gridded objective analysis data from EN4 and other reanalysis products to demonstrate the validity of our results. Figure 7 displays the root mean square error (RMSE) of the temperature in the analysis fields for the period of 2008–2017 by region. We compared the results to EN4, ORAS4, and ECDA. The regions are global (within 66.5° N–S), Pacific, Indian Ocean, Atlantic, and intra-tropical (within 30° N–S). Similar findings can be observed globally and in most regions using different datasets. When examining the global mean temperature, the depths with significant analysis errors are consistent with the parameter-sensitive depths, indicating that parameter uncertainty can impact the analysis accuracy. Moreover, the reduced RMSEs of the PE experiment indicate that PE improves the quality of the analysis. In particular, noticeable improvements are observed below a depth of 100 m. The most pronounced improvement is observed in the Atlantic Ocean and in tropical regions. Figure 8 illustrates the salinity errors in the analysis. The highest error is observed in the sea surface layer, which is consistent with the depth most sensitive to parameters (Fig. 3b and d). In contrast to temperature,

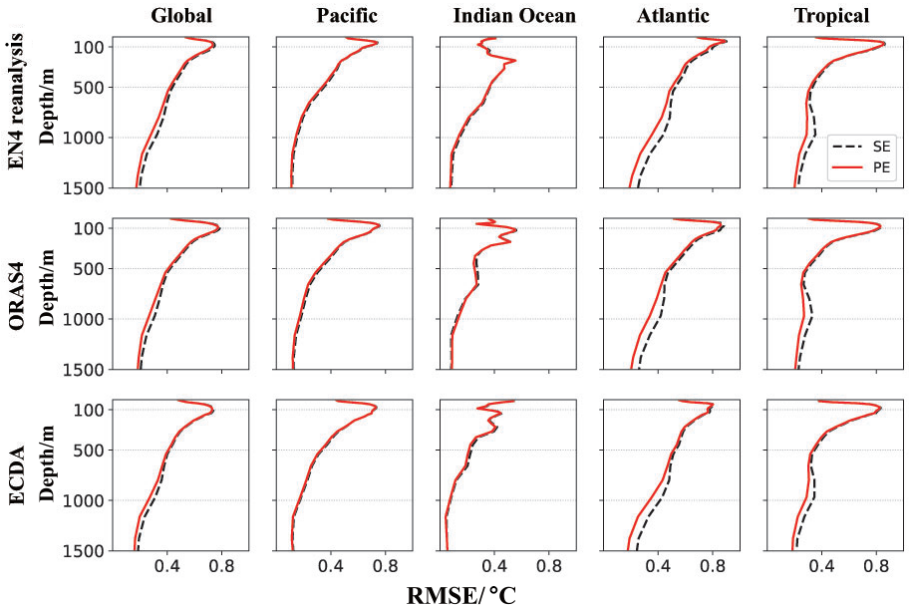

Figure 7. The temperature RMSE of the data assimilation results with EN4 (top), ORAS4 (middle), and ECDA (bottom) for the period of 2008–2017 by region. The regions are as follows: global (within 66.5° N–S), Pacific, Indian Ocean, Atlantic, and intra-tropical (within 30° N–S), from left to right.

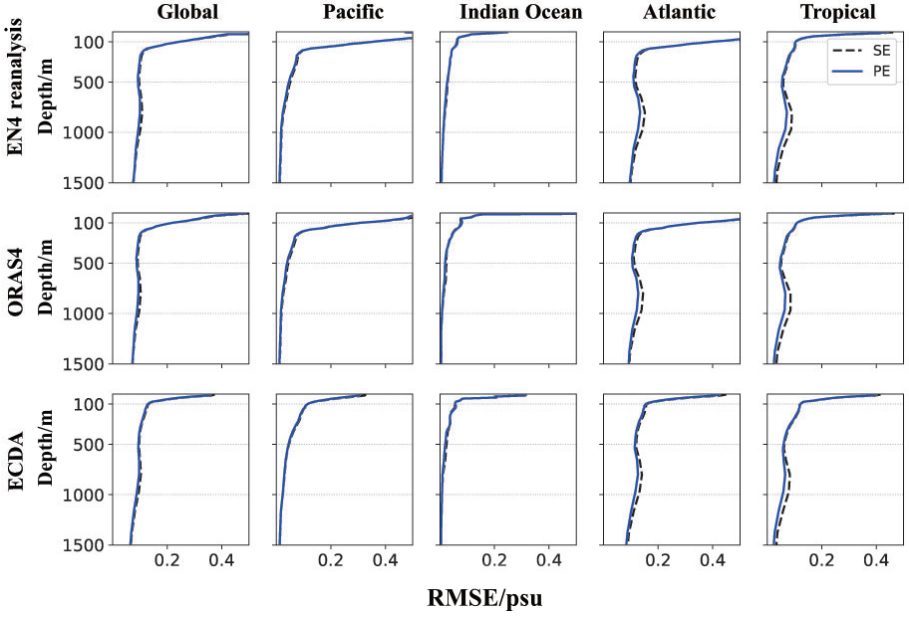

Figure 8. The same as Fig. 7 but for salinity RMSE.

PE primarily enhances salinity accuracy in deep-Atlantic and tropical regions.

Figure 9 displays the RMSEs of the SE experiment and EN4 data in the tropics while emphasizing the disparity compared to the PE experiment. As Fig. 9a shows, the most considerable temperature errors appear in all oceans around the depth of 100 m, which matches the sensitivity analysis result for temperature depicted in Fig. 9c. Figure 9e denotes an improvement in PE for these errors, implying its usefulness throughout the tropics. It is noted that there is improvement in areas where the temperature is sensitive to the uncertainty of those parameters. The temperature error in the deeper layers of the tropical oceans has also been reduced, especially in the deeper Atlantic Ocean. Figure 9b, d, and f show the results for salinity. Although not as significant as temperature, the depths and areas where salinity errors emerge in the SE

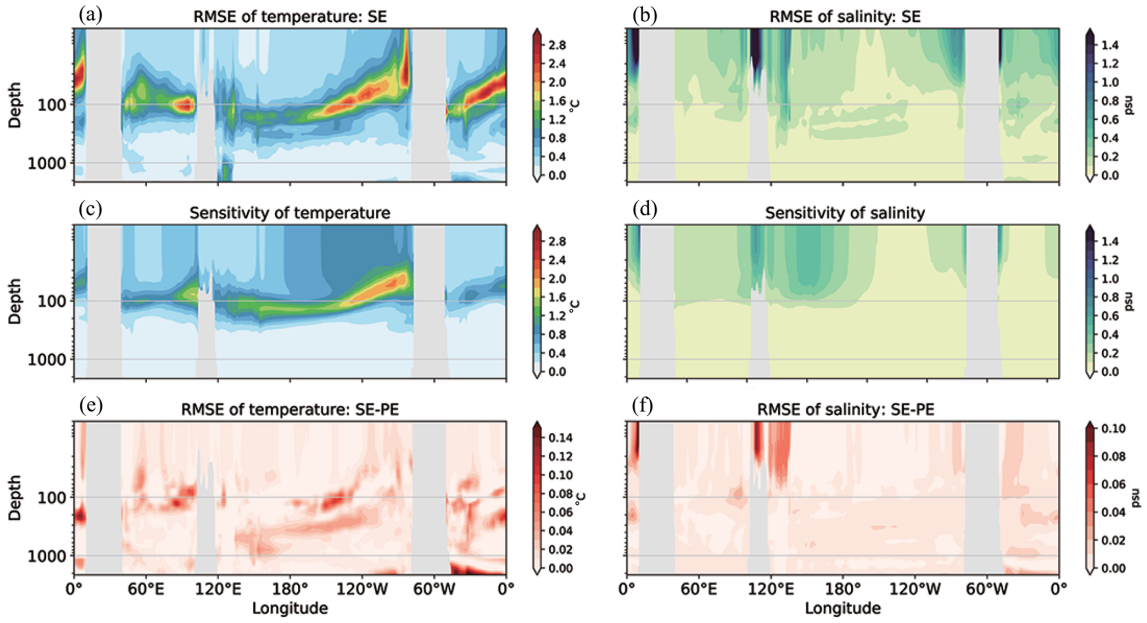

Figure 9. The temperature **(a)** and salinity **(b)** RMSEs of the SE results and EN4 data in the tropics; the mean temperature **(c)** and salinity **(d)** spreads of the sensitivity experiment results in the tropics; the difference between the temperature **(e)** and salinity **(f)** RMSEs of the SE results and those of the PE results, respectively.

analysis align with those sensitive to parameters. Unsurprisingly, PE partially mitigates these errors, most significantly around the Andaman Sea, in waters near Indonesia, and in the coastal West African waters where vertical mixing is intensive.

The model bias of CESM is relatively large in the Atlantic Ocean. Danabasoglu et al. (2012) have shown the zonal-mean temperature and salinity of CCSM4 (which uses the same ocean model as CESM) minus climatology from observations. They noted that the deep Atlantic Ocean remains generally warmer than observed by about 0.58 °C in terms of the mean. The local temperature and salinity maxima between 20 and 30° N at a depth of about 1000 m are associated with the warmer- and saltier-than-observed Mediterranean outflow through the Strait of Gibraltar. The largest salty biases occur in the deep Atlantic Ocean. The upper-ocean Atlantic north of 15° N remains mostly saltier than the climatology. We show similar results in Fig. 10, which displays the zonal-mean temperature and salinity of the Atlantic minus the climatology calculated from EN4 data using SE results and PE results, respectively. By comparing the climatology bias of the results from two experiments, it is seen that the most significant improvement in the PE in relation to the SE lies in the Atlantic Ocean at a depth of 1000 m between 20 and 30° N. It strongly suggests the contribution of improved background diffusivity parameters to reducing model systematic biases. It can be inferred from the conclusions of Danabasoglu et al. (2012) that this improvement also stems from the improvement in the outward flow in the Strait of Gibraltar. Although the sensitivity and analytical errors in this region cannot be demonstrated directly in Fig. 9 due to resolution, the effect of PE is demonstrated by affecting the 1000 m Atlantic Ocean between 20 and 30° N. This explains the smaller deep-Atlantic RMSE in the PE results presented in Figs. 7 and 8.

3.4 ENSO forecast experiment

This study utilized analysis ensembles from the coupled data assimilation system to conduct ENSO forecast experiments between 2008 and 2017 (as shown in the schematic diagram in Fig. 2b and c). The Niño 3.4 index, calculated as the averaged sea surface temperature anomalies between the latitudes of 5° S to 5° N and longitudes of 190° E to 120° W, was employed to illustrate the variability of ENSO. The Niño 3.4 indices of the SE and PE forecasts were computed against various lead times. The anomaly correlation coefficients (ACCs) of these outcomes with the index derived from HadISST data were employed to measure the prediction skills, as shown in Fig. 11a. Moreover, Fig. 11b depicts the RMSE of the forecasts against HadISST.

The prediction skills of both the SE and PE cases were significantly superior to those of the persistence skills represented by a dotted black line. For lead times exceeding 5 months, the PE case exhibited higher ACCs compared to the SE case. By setting the threshold value of an effective prediction as a ACC of 0.5, which is equivalent to the 99 % statistical confidence level with an independent sample size of 30, it was observed that the SE case effectively predicted ENSO at a lead time of up to 9 months, which is 1 month in advance

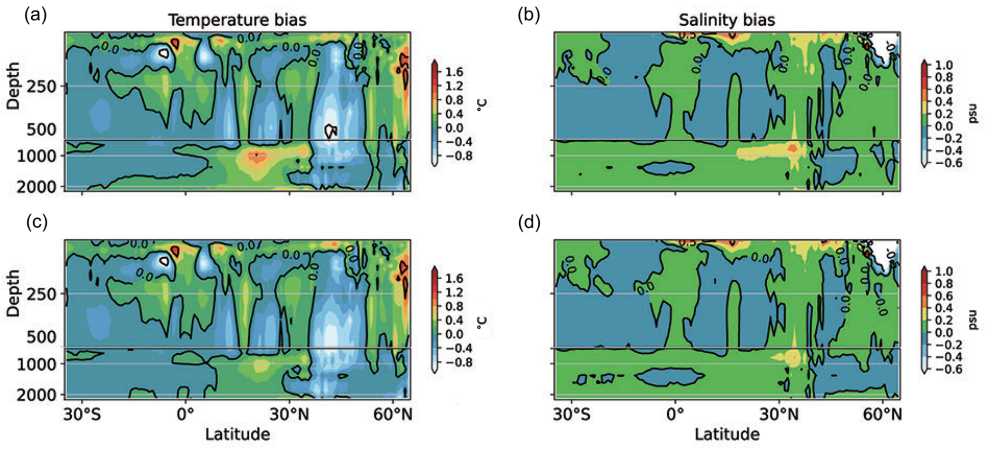

Figure 10. The zonal-mean temperature **(a)** and salinity **(b)** of the Atlantic minus the climatology calculated from EN4 data using the SE results and the zonal-mean temperature **(c)** and salinity **(d)** of the Atlantic bias using the PE results.

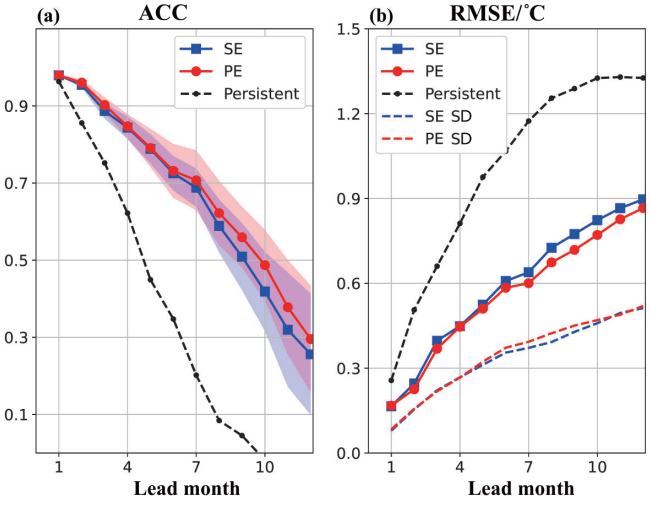

Figure 11. Correlation coefficients **(a)** and root mean square errors (RMSEs) and mean spreads **(b)** of the observed and forecasted Niño 3.4 index as a function of lead time.

compared to the PE case. To demonstrate the significance of the PE advantage, ACCs were computed for each ensemble member using HadISST. The shaded areas represent the ACCs of the ensemble mean plus/minus the standard deviation of the ACCs of each member, further confirming the superior prediction ability of the PE case.

The root mean square errors (RMSEs) of the PE case were also lower than those of the SE case, particularly after a lead time of 5 months. Additionally, the ensemble spreads (dashed colorful lines in Fig. 11b) of the PE results were larger compared to those of the SE predictions. Since the spreads of the PE results were closer to the RMSE than those of the SE results, it is clear that the PE initial conditions are more consistent.

Figure 12 illustrates the spatial correlation coefficient pattern between the predicted sea surface temperature (SST) anomaly and the corresponding HadISST data over the tropical Pacific for the SE and PE cases. The SE and PE results showed no significant difference for lead times of 1 or 4 months. However, for longer lead times, the initial conditions and parameters obtained through PE significantly improved the SST anomaly in the tropical Pacific. As illustrated in Fig. 9, the outcomes of our data assimilation experiments reveal a notable reduction in analysis error within the thermocline of the equatorial Pacific due to parameter estimation. This yields improved initial conditions for ensemble prediction. Simultaneously, the refined parameters contribute to enhanced global vertical mixing. Consequently, the SSTA in the tropical Pacific, derived from our forecasts incorporating parameter estimation, exhibit a higher ACC with observational data. In addition, since the advantage of the PE analysis in the subsurface layer takes some time to affect the SST, the forecast skill based on the PE results is only significantly greater than that of the SE results at longer lead times.

The improvement in PE for ENSO forecasts is likely attributable to better simulations of subsurface temperatures. Previous studies have consistently shown that the accuracy of initial subsurface conditions is crucial for ENSO event prediction (Tang et al., 2003; Song et al., 2022). The PE method not only enhances the accuracy of the initial subsurface conditions (as demonstrated in Figs. 7 and 8) but also provides constrained parameters that more accurately represent the background diffusivity process in the ocean model, leading to improved forecast skills.

4 Conclusions

Errors in the coupled model can arise from uncertainties in the dynamic cores, numerical schemes, physical parameterization schemes, and empirical parameters. PE is the process

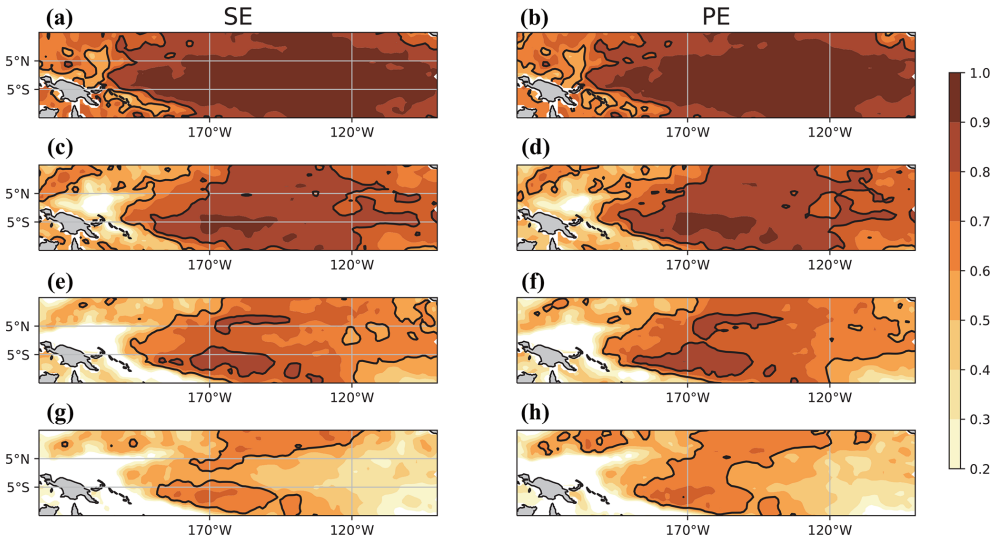

Figure 12. Spatial pattern of the correlation coefficients between the predicted and observed SST anomalies (SSTAs) with SE initialization (left column) and PE initialization (right column) at the 1-month, 4-month, 7-month, and 10-month lead times.

of adjusting or optimizing model parameters using observations; the method of PE is very similar to SE. However, PE has additional complexity since parameters are indirectly related to model states, and the state–parameter covariance is challenging to estimate.

In this study, the fully coupled CESM was used to perform the SE and PE experiments, in which satellite SST and subsurface T–S profiles were assimilated using an ensemble Kalman filter to estimate the model states and critical parameters in vertical mixing parameterization. The SE system was established and comprehensively evaluated by Chen et al. (2022), and PE methods were developed using a new solution to deal with constant parameter evolution (Shen and Tang, 2022). In this work, we used these systems to conduct experiments to compare the SE and PE in the CGCM.

The parameter sensitivity experiments were first conducted to evaluate the sensitivity of the model variables to the parameters, which were measured by the ensemble spread for the temperature and salinity variables. Figures 3 and 4 show that the BVDCs impact the model temperature and salinity variables significantly. Therefore, the PE is theoretically feasible using SST and T–S observations.

However, in this work, we intentionally do not use the CCI method and let the parameter ensemble degenerate in the PE experiment. At this point, all ensemble members can use the same improved parameters to carry out the ensemble forecast, which makes the ensemble forecast easier to carry out and compare with other schemes. This may not be the optimal solution for parameter estimation, but it is the most convenient solution for carrying out realistic forecasts. The experiment in Shen and Tang (2022) also assimilates synthetic T–S profiles and SST observations to estimate the vdc1 parameter in the same CESM model. As shown in their Fig. 10, the amount of change in the parameter values after a period of assimilation is very small as long as the proper parameter covariance inflation coefficients are used (scenarios a–c), so we believe that switching off the CCI also yields relatively improved parameters.

The data assimilation results, using either SE or PE, were assessed against the EN4 objective analysis dataset and the other reanalysis datasets. The DA analysis errors (Figs. 7–10) and the parameter sensitivity results have similar patterns, ultimately revealing that the model errors were partly caused by uncertainties in these parameters. PE can reduce analysis errors in sensitive domains by considering the parameter uncertainties during assimilation.

One key challenge of using PE with real observations is the verification of the parameters, which cannot be observed. In this study, the estimated parameters and PE-derived initial conditions are employed to perform ensemble ENSO prediction. The prediction outcomes provide evidence of the benefits of using PE. Figures 11 and 12 present evidence that using more accurate initial conditions and better parameters in the PE method increases the prediction skill of ENSO, which further verifies our conclusions.

This study brings forward the advancement of PE studies, from the perfect Observing System Simulation Experiment (OSSE) model scenario to real-world-observation assimilation in CGCMs. The comparison between PE and SE highlights the potential of PE to improve coupled model reanalysis and prediction. However, the results in Figs. 11 and 12 indicate that PE only slightly improves the prediction skill of this coupled prediction system. However, the prediction skill of ENSO is affected by many factors, such as predictability, in addition to the initial conditions and model errors (Liu et al., 2022). Therefore, every bit of improvement in the

ENSO dynamical prediction skill is of some practical significance. Nevertheless, we will also pursue higher dynamical prediction skill in future research.

In addition, to reduce the complexity of the problem, we only estimated four parameters in the vertical mixing parameterization in this study. However, many parameters in various physical processes exist that have impacts on the simulation and prediction of ENSO (Gao and Zhang, 2017; Zhao et al., 2019), which should be considered in future studies. Moreover, the spatial distribution of the parameter sensitivity, as shown in Fig. 3, has not been used in the PE algorithm. This may serve as a potential strategy (Shen et al., 2022) to improve the efficiency of PE methods in CGCMs.

Code and data availability. The data used for assimilation and validation in this study can be accessed online from the following sources: World Ocean Atlas 2018 (WOA18) (https://www.ncei.noaa.gov/access/world-ocean-atlas-2018, last access: 18 April 2021, Garcia et al., 2019), the Optimum Interpolation Sea Surface Temperature (OISST) dataset (ftp://eclipse.ncdc.noaa.gov/pub/OI-daily-v2/NetCDF-uncompress, last access: 14 January 2022, Huang et al., 2021), EN4 (https://www.metoffice.gov.uk/hadobs/en4/download-en4-2-1.html, last access: 19 October 2021, Good et al., 2013), the Hadley Centre sea ice and sea surface temperature dataset (HadISST) (https://www.metoffice.gov.uk/hadobs/hadisst, last access: 18 January 2022; Rayner et al., 2003), the Geophysical Fluid Dynamics Laboratory's ensemble coupled data assimilation (GFDL/ECDA) (https://www.gfdl.noaa.gov/ocean-data-assimilation-model-output/, last access: 12 October 2021, Zhang et al., 2007), and the Ocean Reanalysis System 4 (ORAS4) (https://www.ecmwf.int/en/research/climate-reanalysis/ocean-reanalysis, ast access: 12 October 2021, Balmaseda et al., 2013).

The Community Earth System Model (CESM v1.2.1) and the Data Assimilation Research Testbed (DART), both utilized and modified in this study for parameter estimation, are archived on Zenodo under the following DOI: https://doi.org/10.5281/zenodo.8115394 (Shen, 2023). The repository also includes the experiment results and the scripts for plotting.

Author contributions. ZS: conceptualization, methodology, writing – original draft and editing. YC: methodology, experiment. XL: writing – review and editing. XS: methodology, experiment.

Competing interests. The contact author has declared that none of the authors has any competing interests.

Disclaimer. Publisher's note: Copernicus Publications remains neutral with regard to jurisdictional claims made in the text, published maps, institutional affiliations, or any other geographical representation in this paper. While Copernicus Publications makes every effort to include appropriate place names, the final responsibility lies with the authors.

Acknowledgements. The authors thank the editor, Qiang Wang, reviewer Shiqiu Peng, and one anonymous referee for their helpful and constructive comments on the paper.

Financial support. This research has been supported by the National Natural Science Foundation of China (grant no. 42176003), the Fundamental Research Funds for the Central Universities (grant no. B210201022), and the Jiangsu Provincial Innovation and Entrepreneurship Doctor Program (grant no. JSSCBS20210252).

Review statement. This paper was edited by Qiang Wang and reviewed by Shiqiu Peng and one anonymous referee.

References

Aksoy, A., Zhang, F., and Nielsen-Gammon, J. W.: Ensemble-based simultaneous state and parameter estimation with MM5, Geophys. Res. Lett., 33, L12801, https://doi.org/10.1029/2006GL026186, 2006.

Anderson, J. L.: A local least squares framework for ensemble filtering, Mon. Weather Rev., 131, 634–642, 2003.

Anderson, J. L., Hoar, T. J., Raeder, K., Liu, H., Collins, N., Torn, R. D., and Avellano, A.: The Data Assimilation Research Testbed: A Community Facility, B. Am. Meteorol. Soc., 90, 1283–1296, 2009.

Annan, J.: Parameter estimation using chaotic time series, Tellus A, 57, 709–714, 2005.

Annan, J. D. and Hargreaves, J. C.: Efficient parameter estimation for a highly chaotic system, Tellus A, 56, 520–526, 2004.

Balmaseda, M., Alves, O., Arribas, A., Awaji, T., Behringer, D., Ferry, N., Fujii, Y., Lee, T., Rienecker, M., Rosati, T., and Stammer, D.: Ocean Initialization for Seasonal Forecasts, Oceanography, 22, 154–159, https://doi.org/10.5670/oceanog.2009.73, 2009.

Balmaseda, M., Mogensen, K., and Weaver, A.: Evaluation of the ECMWF ocean reanalysis system ORAS4, Q. J. Roy. Meteor. Soc., 139, 1132–1161, 2013.

Bryan, F.: Parameter sensitivity of primitive equation ocean general circulation models, J. Phys. Ocean, 17, 970–985, 1987.

Chen, Y., Shen, Z., and Tang, Y.: On Oceanic Initial State Errors in the Ensemble Data Assimilation for a Coupled General Circulation Model, J. Adv. Model. Earth Sy., 14, e2022MS003106, https://doi.org/10.1029/2022MS003106, 2022.

Chen, Y., Shen, Z., Tang, Y., and Song, X.: Ocean data assimilation for the initialization of seasonal prediction with the Community Earth System Model, Ocean Modell., 183, 102194, https://doi.org/10.1016/j.ocemod.2023.102194, 2023.

Cheng, L. and Kitade, Y.: Quantitative evaluation of turbulent mixing in the Central Equatorial Pacific, J. Oceanogr., 70, 63–79, 2014.

Danabasoglu, G., Bates, S. C., Briegleb, B. P., Jayne, S. R., Jochum, M., Large, W. G., Peacock, S., and Yeager, S. G.: The CCSM4 Ocean Component, J. Climate, 25, 1361–1389, 2012.

Evensen, G., Dee, D. P., and Schröter, J.: Parameter Estimation in Dynamical Models, vol. 516 of NATO Science Series, Springer,

Dordrecht, 373–398, https://doi.org/10.1007/978-94-011-5096-5, 1998.

Fujii, Y., Nakaegawa, T., Matsumoto, S., Yasuda, T., Yamanaka, G., and Kamachi, M.: Coupled Climate Simulation by Constraining Ocean Fields in a Coupled Model with Ocean Data, J. Climate, 22, 5541–5557, https://doi.org/10.1175/2009JCLI2814.1, 2009.

Gao, C. and Zhang, R.-H.: The roles of atmospheric wind and entrained water temperature (Te) in the second-year cooling of the 2010–12 La Niña event, Clim. Dynam., 48, 597–617, 2017.

Gao, Y., Tang, Y., Song, X., and Shen, Z.: Parameter Estimation Based on a Local Ensemble Transform Kalman Filter Applied to El Niño–Southern Oscillation Ensemble Prediction, Remote Sens., 13, 3923, https://doi.org/10.3390/rs13193923, 2021.

Garcia, H., Boyer, T., Baranova, O., Locarnini, R., Mishonov, A., Grodsky, A. E., Paver, C., Weathers, K., Smolyar, I., Reagan, J., Seidov, D., and Zweng, M.: World ocean atlas 2018: Product documentation, edited by: Mishonov, A., 1, 1–20, https://www.ncei.noaa.gov/sites/default/files/2022-06/woa18documentation.pdf (last access: 18 April 2021), 2019.

Gaspari, G. and Cohn, S.: Construction of correlation functions in two and three dimensions, Q. J. Roy. Meteor. Soc., 125, 723–757, 1999.

Good, S. A., Martin, M. J., and Rayner, N. A.: EN4: Quality controlled ocean temperature and salinity profiles and monthly objective analyses with uncertainty estimates, J. Geophys. Res.-Oceans, 118, 6704–6716, 2013.

Gouretski, V. and Reseghetti, F.: On depth and temperature biases in bathythermograph data: Development of a new correction scheme based on analysis of a global ocean database, Deep-Sea Res. Pt. I, 57, 812–833, 2010.

Gregg, M. C.: Variations in the Intensity of Small-Scale Mixing in the Main Thermocline, J. Phys. Oceanogr., 7, 436–454, 1977.

Gregg, M. C., Sanford, T. B., and Winkel, D. P.: Reduced mixing from the breaking of internal waves in equatorial waters, Nature, 422, 513–515, 2003.

Han, G., Wu, X., Zhang, S., Liu, Z., and Li, W.: Error Covariance Estimation for Coupled Data Assimilation Using a Lorenz Atmosphere and a Simple Pycnocline Ocean Model, J. Climate, 26, 10218–10231, https://doi.org/10.1175/JCLI-D-13-00236.1, 2013.

Hu, X.-M., Zhang, F., and Nielsen-Gammon, J. W.: Ensemble-based simultaneous state and parameter estimation for treatment of mesoscale model error: A real-data study, Geophys. Res. Lett., 37, L08802, https://doi.org/10.1029/2010GL043017, 2010.

Huang, B., Liu, C., Banzon, V., Freeman, E., Graham, G., Hankins, B., Smith, T., and Zhang, H.: Improvements of the daily optimum interpolation sea surface temperature (DOISST) version 2.1, J. Climate, 34, 8, 2923–2939, https://doi.org/10.1175/JCLI-D-20-0166.1, 2021.

Jin, E. K., Kinter, J. L., Wang, B., Park, C.-K., Kang, I.-S., Kirtman, B. P., Kug, J.-S., Kumar, A., Luo, J.-J., Schemm, J., Shukla, J., and Yamagata, T.: Current status of ENSO prediction skill in coupled ocean–atmosphere models, Clim. Dynam., 31, 647–664, https://doi.org/10.1007/s00382-008-0397-3, 2008.

Jochum, M.: Impact of latitudinal variations in vertical diffusivity on climate simulations, J. Geophys. Res., 114, C01010, https://doi.org/10.1029/2008JC005030, 2009.

Jochum, M. and Potemra, J.: Sensitivity of tropical rainfall to Banda Sea diffusivity in the community climate system model, J. Climate, 21, 6445–6454, 2008.

Karspeck, A. R., Danabasoglu, G., Anderson, J., Karol, S., Collins, N., Vertenstein, M., Raeder, K., Hoar, T., Neale, R., Edwards, J., and Craig, A.: A global coupled ensemble data assimilation system using the Community Earth System Model and the Data Assimilation Research Testbed, Q. J. Roy. Meteor. Soc., 144, 2404–2430, 2018.

Kivman, G. A.: Sequential parameter estimation for stochastic systems, Nonlin. Processes Geophys., 10, 253–259, https://doi.org/10.5194/npg-10-253-2003, 2003.

Kondrashov, D., Sun, C., and Ghil, M.: Data Assimilation for a Coupled Ocean–Atmosphere Model. Part II: Parameter Estimation, Mon. Weather Rev., 136, 5062–5076, https://doi.org/10.1175/2008MWR2544.1, 2008.

Kug, J.-S., Kang, I.-S., and Choi, D.-H.: Seasonal climate predictability with Tier-one and Tier-two prediction systems, Clim. Dynam., 31, 403–416, https://doi.org/10.1007/s00382-007-0264-7, 2008.

Kunze, E., Firing, E., Hummon, J. M., Chereskin, T. K., and Thurnherr, A. M.: Global Abyssal Mixing Inferred from Lowered ADCP Shear and CTD Strain Profiles, J. Phys. Oceanogr., 36, 1553–1576, 2006.

Large, W. G., Mcwilliams, J. C., and Doney, S. C.: Oceanic vertical mixing: A review and a model with a nonlocal boundary layer parameterization, Rev. Geophys., 32, 363–403, 1994.

Ledwell, J. R., Watson, A. J., and Law, C. S.: Mixing of a tracer in the pycnocline, J. Geophys. Res.-Oceans, 103, 21499–21529, 1998.

Liu, T., Song, X., Tang, Y., Shen, Z., and Tan, X.: ENSO predictability over the past 137 years based on a CESM ensemble prediction system, J. Climate, 35, 763–777, https://doi.org/10.1175/JCLI-D-21-0450.1, 2022.

Liu, Y., Liu, Z., Zhang, S., Jacob, R., Lu, F., Rong, X., and Wu, S.: Ensemble-Based Parameter Estimation in a Coupled General Circulation Model, J. Climate, 27, 7151–7162, 2014a.

Liu, Y., Liu, Z., Zhang, S., Rong, X., Jacob, R., Wu, S., and Lu, F.: Ensemble-based parameter estimation in a coupled GCM using the adaptive spatial average method, J. Climate, 27, 4002–4014, 2014b.

MacKinnon, J. and Winters, K.: Subtropical catastrophe: Significant loss of low-mode tidal energy at 28.9°, Geophys. Res. Lett., 32, L15605, https://doi.org/10.1029/2005GL023376, 2005.

Menemenlis, D., Fukumori, I., and Lee, T.: Using Green's Functions to Calibrate an Ocean General Circulation Model, Mon. Weather Rev., 133, 1224–1240, https://doi.org/10.1175/MWR2912.1, 2005.

Mulholland, D. P., Laloyaux, P., Haines, K., and Balmaseda, M. A.: Origin and Impact of Initialization Shocks in Coupled Atmosphere–Ocean Forecasts*, Mon. Weather Rev., 143, 4631–4644, https://doi.org/10.1175/MWR-D-15-0076.1, 2015.

Munk, W. H.: Abyssal recipes, Deep-Sea Res. Ocean. Abstr., 13, 707–730, https://doi.org/10.1016/0011-7471(66)90602-4, 1966.

Navon, I.: Practical and theoretical aspects of adjoint parameter estimation and identifiability in meteorology and oceanography, Dynam. Atmos. Oceans, 27, 55–79, 1998.

Neale, R. B., Gettelman, A., Park, S., Conley, A. J., Kinnison, D., Marsh, D., Smith, A. K., Vitt, F., Morrison, H., and Cameron-

smith, P.: Description of the NCAR Community Atmosphere Model (CAM 5.0), Natl. Cent. for Atmos, Land Model, Tech. Note NCAR/TN-486+STR, 2010.

Penny, S. G. and Hamill, T. M.: Coupled Data Assimilation for Integrated Earth System Analysis and Prediction, B. Am. Meteorol. Soc., 98, ES169–ES172, https://doi.org/10.1175/BAMS-D-17-0036.1, 2017.

Rayner, N., Parker, D. E., Horton, E., Folland, C. K., Alexander, L. V., Rowell, D., Kent, E. C., and Kaplan, A.: Global analyses of sea surface temperature, sea ice, and night marine air temperature since the late nineteenth century, J. Geophys. Res.-Atmos., 108, 4407, https://doi.org/10.1029/2002JD002670, 2003.

Shen, Z.: Data and code for gmd-2023-113 "Parameter estimation for ocean background vertical diffusivity coefficients in the Community Earth System Model (v1.2.1) and its impact on ENSO forecast", Zenodo [code and data set], https://doi.org/10.5281/zenodo.8115394, 2023.

Shen, Z. and Tang, Y.: A two-stage inflation method in parameter estimation to compensate for constant parameter evolution in Community Earth System Model, Acta Oceanol. Sin., 41, 1–12, https://doi.org/10.1007/s13131-021-1856-5, 2022.

Shen, Z., Zhong, Q., and Chen, Z.: Parameter estimation using adaptive observations towards maximum total variance reduction with ensemble adjustment Kalman filter, Front. Climate, 4, 850386, https://doi.org/10.3389/fclim.2022.850386, 2022.

Smith, R., Dukowicz, J., and Malone, R.: Parallel ocean general circulation modeling, Phys. D, 60, 38–61, 1992.

Smith, R., Jones, P., Briegleb, B., Bryan, F., Danabasoglu, G., Dennis, J., Dukowicz, J., Eden, C., Fox-Kemper, B., Gent, P., Hecht, M., Jayne, S., Jochum, M., Large, W., Lindsay, K., Maltrud, M., Norton, N., Peacock, S., Vertenstein, M., and Yeager, S.: The Parallel Ocean Program (POP) Reference Manual, LAUR-01853, 141, 1–140, 2010.

Song, X., Li, X., Zhang, S., Li, Y., Chen, X., Tang, Y., and Chen, D.: A new nudging scheme for the current operational climate prediction system of the National Marine Environmental Forecasting Center of China, Acta Oceanol. Sin., 41, 51–64, https://doi.org/10.1007/s13131-021-1857-4, 2022.

Stammer, D., Balmaseda, M., Heimbach, P., Köhl, A., and Weaver, A.: Ocean data assimilation in support of climate applications: Status and perspectives, Annu. Rev. Mar. Sci., 8, 491–518, 2016.

Tang, Y., Kleeman, R., Moore, A. M., Weaver, A., and Vialard, J.: The use of ocean reanalysis products to initialize ENSO predictions: initialization of ENSO prediction, Geophys. Res. Lett., 30, 1694, https://doi.org/10.1029/2003GL017664, 2003.

Tong, M. and Xue, M.: Simultaneous Estimation of Microphysical Parameters and Atmospheric State with Simulated Radar Data and Ensemble Square Root Kalman Filter. Part II: Parameter Estimation Experiments, Mon. Weather Rev., 136, 1649–1668, https://doi.org/10.1175/2007MWR2071.1, 2008a.

Tong, M. and Xue, M.: Simultaneous Estimation of Microphysical Parameters and Atmospheric State with Simulated Radar Data and Ensemble Square Root Kalman Filter. Part I: Sensitivity Analysis and Parameter Identifiability, Mon. Weather Rev., 136, 1630–1648, https://doi.org/10.1175/2007MWR2070.1, 2008b.

Wu, X., Zhang, S., Liu, Z., Rosati, A., Delworth, T. L., and Liu, Y.: Impact of Geographic-Dependent Parameter Optimization on Climate Estimation and Prediction: Simulation with an Intermediate Coupled Model, Mon. Weather Rev., 140, 3956–3971, https://doi.org/10.1175/MWR-D-11-00298.1, 2012.

Wu, X., Han, G., Zhang, S., and Liu, Z.: A study of the impact of parameter optimization on ENSO predictability with an intermediate coupled model, Clim. Dynam., 46, 711–727, 2016.

Zhang, S., Harrison, M., Rosati, A., and Wittenberg, A.: System design and evaluation of coupled ensemble data assimilation for global oceanic climate studies, Mon. Weather Rev., 135, 3541–3564, 2007.

Zhang, S., Liu, Z., Rosati, A., and Delworth, T.: A study of enhancive parameter correction with coupled data assimilation for climate estimation and prediction using a simple coupled model, Tellus A, 64, 10963, https://doi.org/10.3402/tellusa.v64i0.10963, 2012.

Zhang, S., Liu, Z., Zhang, X., Wu, X., and Deng, X.: Coupled data assimilation and parameter estimation in coupled ocean–atmosphere models: a review, Clim. Dynam., 54, 5127–5144, https://doi.org/10.1007/s00382-020-05275-6, 2020.

Zhao, Y., Liu, Z., Zheng, F., and Jin, Y.: Parameter Optimization for Real-World ENSO Forecast in an Intermediate Coupled Model, Mon. Weather Rev., 147, 1429–1445, https://doi.org/10.1175/MWR-D-18-0199.1, 2019.

Zhu, Y. and Zhang, R. H.: An Argo-Derived Background Diffusivity Parameterization for Improved Ocean Simulations in the Tropical Pacific, Geophys. Res. Lett., 45, 1509–1517, 2018.